BIOMICROFLUIDICS **10**, 034119 (2016)

Acoustofluidic harvesting of microalgae on a single chip

Jee-Woong Park,[1] Soo Hyeon Kim,[2] Takuro Ito,[3] Teruo Fujii,[2] So Youn Kim,[4] Thomas Laurell,[4,5] Sang Wook Lee,[1,a)] and Keisuke Goda[1,6,7,b)]
[1]*Department of Chemistry, University of Tokyo, Tokyo 113-0033, Japan*
[2]*Institute of Industrial Science, University of Tokyo, Tokyo 153-8505, Japan*
[3]*Institute for Advanced Biosciences, Keio University, Tsuruoka 997-0035, Japan*
[4]*Department of Biomedical Engineering, Dongguk University, Seoul, South Korea*
[5]*Department of Biomedical Engineering, Lund University, 221 00 Lund, Sweden*
[6]*Department of Electrical Engineering, University of California, Los Angeles, California 90095, USA*
[7]*Japan Science and Technology Agency, Tokyo 102-0076, Japan*

(Received 31 March 2016; accepted 13 June 2016; published online 22 June 2016)

We present an on-chip acoustofluidic platform for harvesting a target microalgal species from a heterogeneous population of cells and particles based on their size, density, and compressibility in a rapid, non-invasive, energy-efficient, continuously running, and automated manner. For our proof-of-principle demonstration, we use *Euglena gracilis* as a target species. Specifically, we show the simultaneous separation and enrichment of *E. gracilis* from a mixed population of *E. gracilis* in pond water (consisting of other microalgae and various kinds of particles as contaminants) on a single acoustofluidic chip with a recovery ratio of 92.6%, a target separation ratio of 90.1%, a concentration factor of 3.43, an enrichment factor of 12.76, and a cell viability rate of 98.3% at a high volume rate of 500 μl/min. Our results indicate that the on-chip acoustofluidic platform is an effective tool for harvesting target microalgae from mixed populations of microalgae and other contaminants. *Published by AIP Publishing.* [http://dx.doi.org/10.1063/1.4954744]

I. INTRODUCTION

Microalgal biofuel is a promising alternative to liquid fossil fuels due to their advantages over the first and second generation biofuels[1,2] and has, thereby, gained much attention from both the academic and industrial sectors over the last decade.[3,4] It is based on microalgae as a source of carbon-neutral oils in the form of triacylglycerol molecules.[5] Microalgae grow in a diverse range of aquatic environments ranging from freshwater to saturated saline and efficiently absorb atmospheric CO_2 via photosynthesis and are responsible for over 40% of the global carbon fixation.[6] Compared with traditional terrestrial crops such as corn, soybeans, and canola, microalgae such as *Botryococcus braunii*, *Chlorella*, and *Euglena gracilis* grow rapidly with a typical cell doubling time of 24 h and have a higher oil content (20%–80% in dry weight).[6,7] Consequently, microalgae can provide a much higher biomass production yield (10–100 times higher) despite their need for less water and food, reaching ~100 000 gallons of biofuel per acre per year.[1,8] For harvesting such microalgae from environmental samples, cultivation ponds, or photobioreactors, methods for sampling, isolating, and purifying target microalgae and their unique strains are of prominent importance, but are required to overcome a number of technical challenges before they can be broadly deployed in the competitive fuel market.[9,10]

Unfortunately, conventional harvesting methods are not cost-effective as they involve time- and energy-consuming procedures such as filtration, chemical flocculation, centrifugation, and a combination of any of these before drying.[11,12] Since nearly 30% of the total biofuel production

[a)]sangwook_l@chem.s.u-tokyo.ac.jp
[b)]goda@chem.s.u-tokyo.ac.jp

cost comes from the harvesting process, the high cost of the conventional harvesting methods is currently a factor that limits the commercial use of microalgae for biofuel.[13,14] Specifically, filtration is used to remove macroscopic contaminants such as insects, grains of sand, and pieces of plant leaves from environmental samples and cultivated microalgae in the open,[1] but involves large filtration systems and high operation costs to avoid clogging.[15] Chemical flocculation is a method for forming aggregates to separate contaminants, but is not suitable for handling large sample volumes due to its slow process as well as the high cost of flocculants.[16] Centrifugation, the most commonly used method for harvesting microalgae, uses the centrifugal force for the sedimentation of microscopic contaminants such as dust particles, bacteria, and unwanted microalgal cells, but it is a batch process and involves high capital and operational costs for large-scale microalgal culture systems.[14,17]

In this study, we propose and experimentally demonstrate an on-chip acoustofluidic platform for harvesting a target microalgal species from a mixed population of microalgae and various kinds of particles as contaminants in a rapid, non-invasive, energy-efficient, continuously running, and automated manner. Acoustofluidics is a method that combines microfluidics and acoustophoresis—a technique for label-free manipulation of particles and cells with acoustic forces whose strength differs, depending on their morphological and mechanical properties.[18–21] It is a viable route to the development of integrated systems for non-contact on-chip manipulation of particles and cells.[4,22] Specifically, our on-chip acoustofluidic platform utilizes acoustic radiation forces in a perfused microfluidic channel to align, separate, and enrich the target microalga based on the cell size, density, and compressibility (Fig. 1(a)). For a proof-of-principle experimental demonstration of the harvesting platform, we use *E. gracilis* as a target microalgal species. *E. gracilis* is a species of unicellular flagellate protists found in freshwater and attractive as it is known to produce wax ester and triacylglycerol within lipid droplets which can be refined to produce kerosene suitable for a jet fuel.[23–26] We show the simultaneous separation and enrichment of *E. gracilis* from a mixed population of *E. gracilis* in pond water with a recovery ratio of 92.6%, a target separation ratio of 90.1%, a concentration factor of 3.43, an enrichment factor of 12.76, and a cell viability rate of 98.3% at a high volume rate of 500 μl/min. By eliminating the time-consuming and costly procedures of the conventional harvesting methods, our platform is expected to be a valuable tool for highly automated harvesting of microalgae-based biomass.

II. MATERIALS AND METHODS

A. Sample preparation

For the optimization of the on-chip acoustofluidic device's fluid operation, we used polystyrene (PS) particles (7516A, Thermo Scientific, USA) of different sizes (6, 16, and 25 μm in diameter) suspended in phosphate buffered saline (PBS) with 0.02% tween-20 added to avoid aggregation. The concentration of the particles is less than 10^7 particles/ml to minimize the effect of acoustic and hydrodynamic interaction forces between particles.[27] For microalgal samples, we used *E. gracilis* NIES-48 and *Mychonastes* aff. *jurisii* TKAC1031 which were provided by the Microbial Culture Collection at National Institute for Environmental Studies (NIES) and Tsuruoka, Keio, Algae Collection (TKAC) at Institute for Advanced Biosciences, Keio University, respectively. The cultures were grown in culture flasks using 20 ml of AF-6 medium at pH 6.6[28,29] under 14:10 Light:Dark cycle illumination (approximately 140 μmol) at 25 °C.

B. Device fabrication

The device shown in Fig. 1(a) was fabricated using the conventional photolithography and etching process.[30,31] The microfluidic channel for acoustophoresis was fabricated on a silicon substrate by anisotropic wet etching in KOH (40 g per 100 ml of H_2O, 80 °C). After etching, the chip was sealed to a glass lid by anodic bonding. The width of the microchannel is 300 μm in the aligning region (step I) and 380 μm in the separation region (step II) while its height is

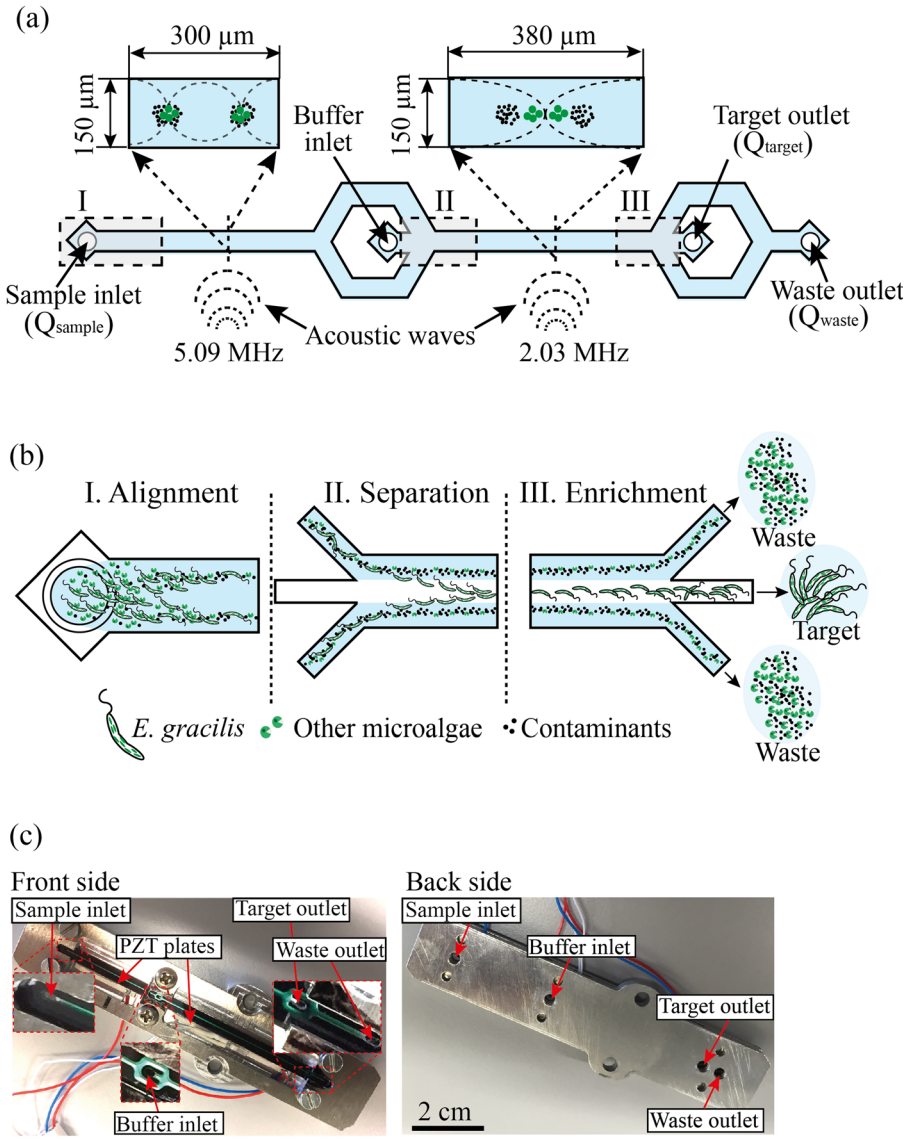

FIG. 1. On-chip acoustofluidic device. (a) Schematic of the device. It consists of two inlets (sample inlet, buffer inlet) and two outlets (target outlet, waste outlet). Cells and particles are first focused into two acoustic pressure nodes by the standing waves at 5.09 MHz. Then, target microalgal cells (*E. gracilis*) are focused into the central acoustic pressure node by the standing waves at 2.03 MHz. The target cells are collected at the target outlet while the other cells and particles are damped at the waste outlet. (b) Functionality of the device. (c) Picture of the constructed device.

150 μm in both regions. The piezoelectric transducers (PZTs) (PZ26, Ferroperm piezoceramics, Denmark) were attached to the silicon chip. The silicon chip was connected to tubes with an inner diameter of 0.01 in. (0.254 mm) glued to the inlets and outlets. The PZTs were actuated through a dual-channel function generator (WF 1974, NF Corporation, Japan) that was amplified by a power amplifier (BA 4850, NF Corporation, Japan). The voltage applied to the PZTs was monitored using an oscilloscope (TDS 2120, Tektronix).

C. Acoustophoresis

The method for our acoustofluidic standing wave manipulation of cells using acoustic radiation pressure is known as acoustophoresis. It enables the separation of cells (including microalgal cells) by size, density, and compressibility using acoustic standing waves in the device's microchannel.[18,32,33] In acoustophoresis, the acoustic radiation force F is applied to cells to

focus them into either pressure nodes or anti-nodes (Fig. 1(a)) and is given by Grenvall *et al.*[34] and Jakobsson *et al.*[35]

$$F = 4\pi a^3 \Phi k E \sin 2kd, \tag{1}$$

where a is the radius of the cell, $k = 2\pi/\lambda$ is the wave vector, E is the acoustic energy density, d is the distance from the wall along the axis of the standing waves, and Φ is the acoustic contrast factor dependent on the density and compressibility of the cells compared to the surrounding medium and is given by Grenvall *et al.*[34] and Jakobsson *et al.*[35]

$$\Phi = \frac{\kappa_o - \kappa_c}{3\kappa_o} + \frac{\rho_c - \rho_o}{2\rho_c + \rho_o}. \tag{2}$$

Here, κ_o is the isothermal compressibility of the surrounding medium, κ_c is the isothermal compressibility of the cell, ρ_o is the density of the surrounding medium, and ρ_c is the density of the cell. As Eq. (1) shows, the acoustic radiation force is linearly proportional to the volume of the cell, a^3, and the contrast factor, Φ. As Eq. (2) shows, if the isothermal compressibility of the cells is identical to that of the surrounding medium, the first term vanishes. Likewise, if the density of the cells is identical to that of the surrounding medium, the second term vanishes.

Acoustofluidic devices employ either bulk acoustic waves (BAWs) or surface acoustic waves (SAWs). In a typical BAW-based device, acoustic standing waves are generated by piezoelectric transducers on the device. Depending on the acoustofluidic channel geometry, the acoustic standing waves at 1–5 MHz can be applied to the liquid in the channel for an efficient manipulation of particles.[18,32] In case of a SAW-based device, acoustic waves are generated by inter-digitated transducers (IDTs) patterned on a piezoelectric plate at 10–1000 MHz.[35] In the device, a microfluidic chamber or channel is placed on the piezoelectric plate for the manipulation of particles in the channel. Comparing the two devices, the BAW-based device is more efficient in dealing with biological cells and similarly sized particles because of the wider frequency range of BAWs. One of the drawbacks of the BAW-based device is its need for highly resonant device designs with low-attenuation materials. Additional active cooling or frequency calibration may be required for the stable operation of acoustic waves against heat-induced perturbations caused by a BAW-induced temperature increase in the device.

D. Device function

The on-chip acoustofluidic device is schematically shown in Fig. 1(a). It consists of a single microchannel, two PZTs bonded on the device which are driven at two different radio frequencies, two inlets (one for infusing the sample into the device and the other for optionally infusing a cell-free liquid as a buffer), a trifurcation-shaped junction, and two outlets (one for collecting the target microalga and the other for discarding the waste). Here, the inlets and outlets are characterized by volume rates at the locations (Q_{sample}, Q_{buffer}, Q_{target}, and Q_{waste}) indicated in Fig. 1(a). As shown in Fig. 1(b), the device simultaneously aligns, separates, and enriches target microalgal cells from the mixed sample by focusing them at the center and unwanted cells and particles near the microchannel walls (see supplementary material, videos 1–5). Fig. 1(c) shows pictures of the front and back of the actual on-chip acoustofluidic device.

In terms of functionality, the acoustofluidic device consists of three regions: alignment, separation, and enrichment. In the alignment region (see supplementary material, videos 1 and 2), the first PZT generates standing waves at a resonance frequency of 5.09 MHz to align the sample into a pair of streams that flow along the sides of the channel. The pressure nodes are located at one quarter of the microchannel width away from each sidewall and at one half of the microchannel height between the bottom of the silicon channel and the top of the glass lid since the 5.09-MHz standing wave matches half a wavelength across the height of the channel (150 μm) and one wavelength across the width of the channel (300 μm). Continuously in the separation region (see supplementary material, videos 3 and 4), the second PZT generates standing waves in the separation channel at a resonance frequency of 2.03 MHz because the

standing wave of 2.03 MHz is identical to half a wavelength across the width of the channel (380 μm) and generates the pressure node at the center of the channel. Because of the significant size difference between the *E. gracilis* and the contaminating particles and cells, the size dependency of the radiation force (Eq. (1)) becomes the dominating factor deciding the net acoustic force while the acoustic contrast factor (Eq. (2)) plays a less pronounced role. Hence, the *E. gracilis* cells from the mixture are directed into the central stream in the microchannel while leaving the smaller unwanted cells and particles in the side streams. Finally, in the enrichment region (see supplementary material, video 5), the side streams are removed at the trifurcation-shaped junction while the central stream is retained.

Optionally, by infusing the buffer into the second inlet, the pre-aligned target cells are hydrodynamically laminated near the sidewalls. While it is not essential and was not used for our experiments below, the buffer can be used to further reduce flow fluctuations and purify the collected sample with a minimal negative effect on the sample.[36]

E. Device evaluation

In order to evaluate the performance of the acoustofluidic device, we used the experimental setup shown in Fig. 2. The flow rates were controlled by syringe pumps (70-4505, Elite pump, Harvard Apparatus, USA) mounted with syringes (SS05-LZ, Terumo, Japan) connected to the inlets and outlets of the microchannel. The inlets and outlets were directly linked to the syringe pumps via peek tubes. In order to avoid the bubble entrapment in the channel, before running the acoustofluidic device, we filled the chip with buffer solution (PBS) by infusing and withdrawing with the syringe pumps. After that, the syringes were replaced with syringes that

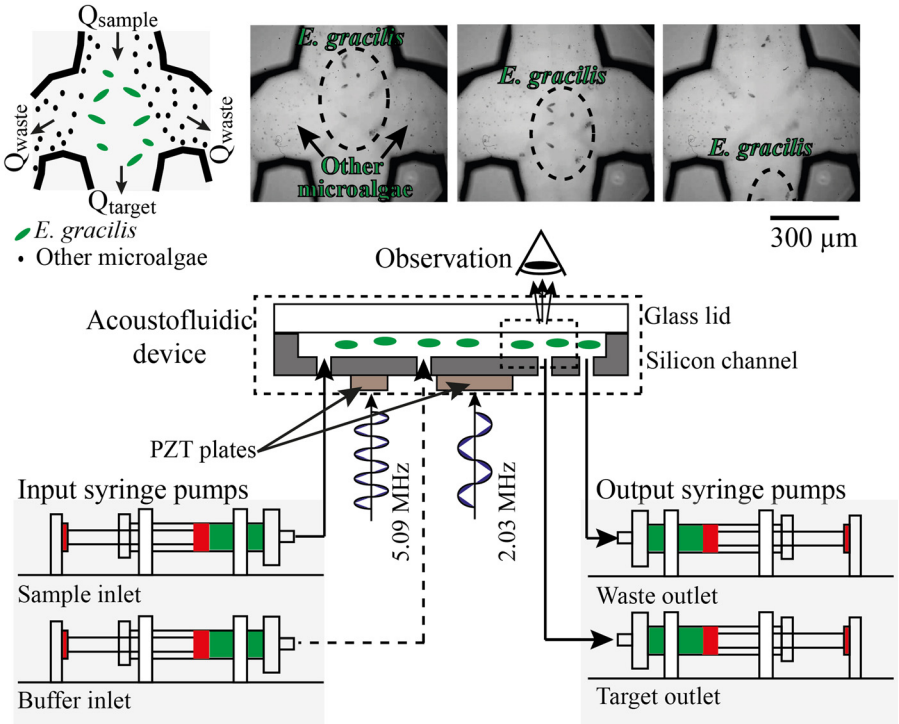

FIG. 2. Evaluation of the on-chip acoustofluidic device. The flow rates were controlled by syringe pumps mounted with syringes connected to the inlets and outlets of the microchannel. The separated cells were enumerated by using an image-based cytometer. The observation of the device's functionality was carried out with a microscope with a high-speed camera at a frame rate of 1200 fps. As a proof-of-principle demonstration, a mixture of *E. gracilis* (50–100 μm sized) and *M.* aff. *jurisii* (5–10 μm sized) was infused into the sample inlet by one of the syringe pumps at a controlled flow rate of 500 μl/min. The sequence of the image frames that capture the dynamical process at the trifurcation-shaped junction in the figure indicates a successful demonstration of directing *E. gracilis* cells into the central channel and *M.* aff. *jurisii* cells and other small particles into the side channels.

contain the liquids for the experiments. The separated cells were enumerated using an image-based cytometer (Invitrogen, Tali, Thermofisher Scientific, USA). The observation of the device's functionality was carried out with a microscope (BX53, Olympus Corporation, Japan) with a high-speed camera at a frame rate of 1200 fps via a 20× objective lens. Our proof-of-principle imaging observation is shown in Fig. 2. Here, a mixture of *E. gracilis* (50–100 μm sized) and *M.* aff. *jurisii* (5–10 μm sized) was infused into the sample inlet by one of the syringe pumps at a controlled flow rate of 500 μl/min. The sequence of the image frames that capture the dynamical process at the trifurcation-shaped junction in the figure indicates a successful demonstration of directing *E. gracilis* cells into the central channel and *M.* aff. *jurisii* cells and other small particles into the side channels.

III. RESULTS AND DISCUSSION

A. Framework for system characterization

The most crucial tasks in medical science and environmental science are efficient separation and enrichment of targeted cells from a mixed sample. Therefore, in order to characterize the performance of the acoustofluidic device, we used the recovery ratio, separation ratio, concentration factor, and enrichment factor defined by the number of target particles in the harvested sample (N_{target}^{out1}) divided by the number of target particles in the original sample (N_{target}^{in}), the number of target particles in the harvested sample (N_{target}^{out1}) divided by the sum of the number of target particles in the harvested sample (N_{target}^{out1}) and the number of target particles in the waste (N_{target}^{out2}), the concentration of target particles in the harvested sample ($N_{\text{target}}^{out1}/V^{\text{out1}}$) divided by the concentration of target particles in the original sample ($N_{\text{target}}^{in}/V^{in}$), and the ratio of the number of target particles to the number of non-target particles in the harvested sample ($N_{\text{target}}^{out1}/N_{\text{non-target}}^{out1}$) divided by the ratio of the number of target particles to the number of non-target particles in the original sample ($N_{\text{target}}^{in}/N_{\text{non-target}}^{in}$), respectively (Fig. 3). More specifically, the parameters are mathematically defined as

$$\text{Recovery ratio} = \frac{N_{\text{target}}^{out1}}{N_{\text{target}}^{in}}, \tag{3}$$

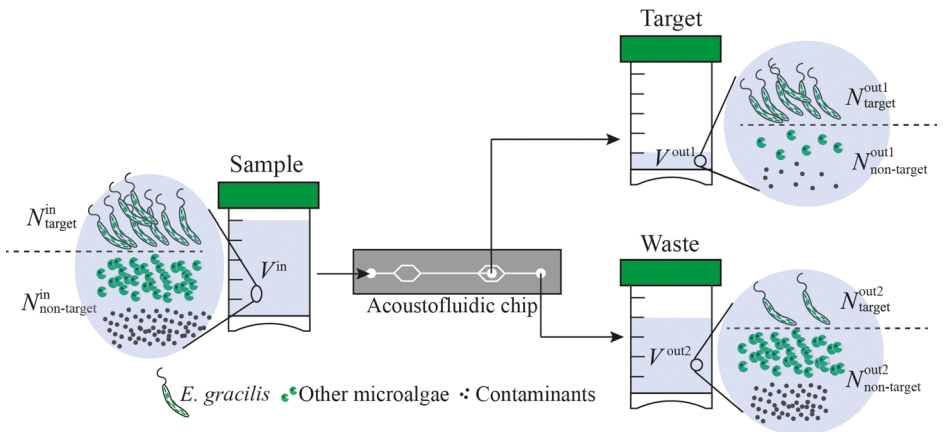

FIG. 3. Definition of the parameters used for the characterization of the on-chip acoustofluidic device. N_{target}^{in} is the number of target particles in the original sample. $N_{\text{non-target}}^{in}$ is the number of non-target particles in the original sample. N_{target}^{out1} is the number of target particles in the harvested sample. $N_{\text{non-target}}^{out1}$ is the number of non-target particles in the harvested sample. N_{target}^{out2} is the number of target particles in the waste. $N_{\text{non-target}}^{out2}$ is the number of non-target particles in the waste. V^{in} is the volume of the sample. V^{out1} is the volume of the harvested sample. V^{out2} is the volume of the waste.

$$\text{Separation ratio} = \frac{N_{\text{target}}^{out1}}{N_{\text{target}}^{out1} + N_{\text{target}}^{out2}}, \tag{4}$$

$$\text{Concentration factor} = \left(\frac{N_{\text{target}}^{out1}}{V^{\text{out1}}}\right) \Big/ \left(\frac{N_{\text{target}}^{in}}{V^{in}}\right), \tag{5}$$

$$\text{Enrichment factor} = \left(\frac{N_{\text{target}}^{out1}}{N_{\text{non-target}}^{out1}}\right) \Big/ \left(\frac{N_{\text{target}}^{in}}{N_{\text{non-target}}^{in}}\right). \tag{6}$$

Here, these parameters depend on the input sample's volume rate (Q_{sample}) and the input buffer's volume rate (Q_{buffer}), as well as the output harvest's volume rate (Q_{target}) and the output waste's volume rate (Q_{waste}).

B. Optimization of the device's harvesting performance

In order to find an optimum condition for the device's harvesting performance, we first used PS particles of 25 μm in diameter as an injection sample since its size is comparable to that of *E. gracilis*. The PS particles were counted using an image cytometer (Invitrogen, Tali, Thermo Fisher Scientific, USA), diluted to a concentration of $\sim 2 \times 10^5$ particles/ml, and infused into the sample inlet port. PS particles were collected at the target outlet while the rest was discarded into the waste outlet (Fig. 1(a)). To find out the optimal fluid operation condition for maximizing the recovery ratio, separation ratio, and concentration factor, we evaluated the device's outlet flow ratio of Q_{target}:Q_{waste} in three different conditions: 1:9 (50 μl/min:450 μl/min), 1:4 (100 μl/min:400 μl/min), and 2:3 (200 μl/min:300 μl/min), respectively, while the input flow rate was maintained at 500 μl/min to achieve the highest possible flow rate.

Fig. 4(a) shows the measured recovery ratio, separation ratio, and concentration factor as a function of the proportion of the number of the particles collected at the target outlet compared to the total number of the collected particles at the target outlet and waste outlet. The concentration factor of the device was measured to be 4.68 ± 0.46 at 1:9, 4.81 ± 0.53 at 1:4, and 2.28 ± 0.03 at 2:3 while the corresponding recovery ratio was $97.8 \pm 1.8\%$, $96.7 \pm 2.3\%$, and $96.6 \pm 3.2\%$, respectively. As the figure shows, there is a large discrepancy in concentration factor between the measured value and our prediction based on the volume fraction, which is due to the central flow's weak drag force in the target outlet tube at 50 μl/min in the case of the output flow ratio of 1:9. Likewise, we obtained the recovery ratio, separation ratio, and concentration factor of *E. gracilis* cells in PBS under the same conditions (Fig. 4(b)) and verified that the optimum conditions are the same for the PS particles and *E. gracilis* cells. The concentration factor of *E. gracilis* cells was measured to be 2.32 ± 0.11 at 1:9, 4.1 ± 0.03 at 1:4, and 2.42 ± 0.29 at 2:3 while the corresponding recovery ratio was $94.2 \pm 4.0\%$, $98.7 \pm 0.8\%$, and $96.0 \pm 2.8\%$, respectively. The best performance of the device was acquired at the outlet flow ratio of 1:4 for both PS particles and *E. gracilis*.

Next, we investigated the recovery ratio, separation ratio, and concentration factor of PS particles at three different input sample flow rates to find the highest flow rate with the highest concentration factor. Just like the investigation above, the concentration factor of PS particles at the fixed output flow ratio of 1:4 was measured to be 2.61 ± 0.12 at 200 μl/min, 4.80 ± 0.52 at 500 μl/min, and 4.26 ± 0.81 at 1000 μl/min with a recovery ratio of $90.8 \pm 0.06\%$, $96.7 \pm 2.3\%$, and 93.3 3.8%, respectively (Fig. 4(c)). Likewise, the concentration factor of *E. gracilis* cells in PBS at the same output flow ratio was measured to be 2.09 ± 0.50 at 200 μl/min, 4.09 ± 0.03 at 500 μl/min, and 3.84 ± 0.90 at 1000 μl/min with a recovery ratio of $96.5 \pm 0.3\%$, $98.7 \pm 0.8\%$, and $96.8 \pm 0.1\%$, respectively (Fig. 4(d)). Both sets of results share a similar trend. Here, the reason why the recovery ratio and hence the concentration factor are reduced at a high flow rate of 1000 μl/min is that the efficiency of focusing the particles and cells into the central acoustic pressure node is decreased due to their reduced retention time in the microchannel. On the other hand, at a low flow rate of 200 μl/min, the particles and cells

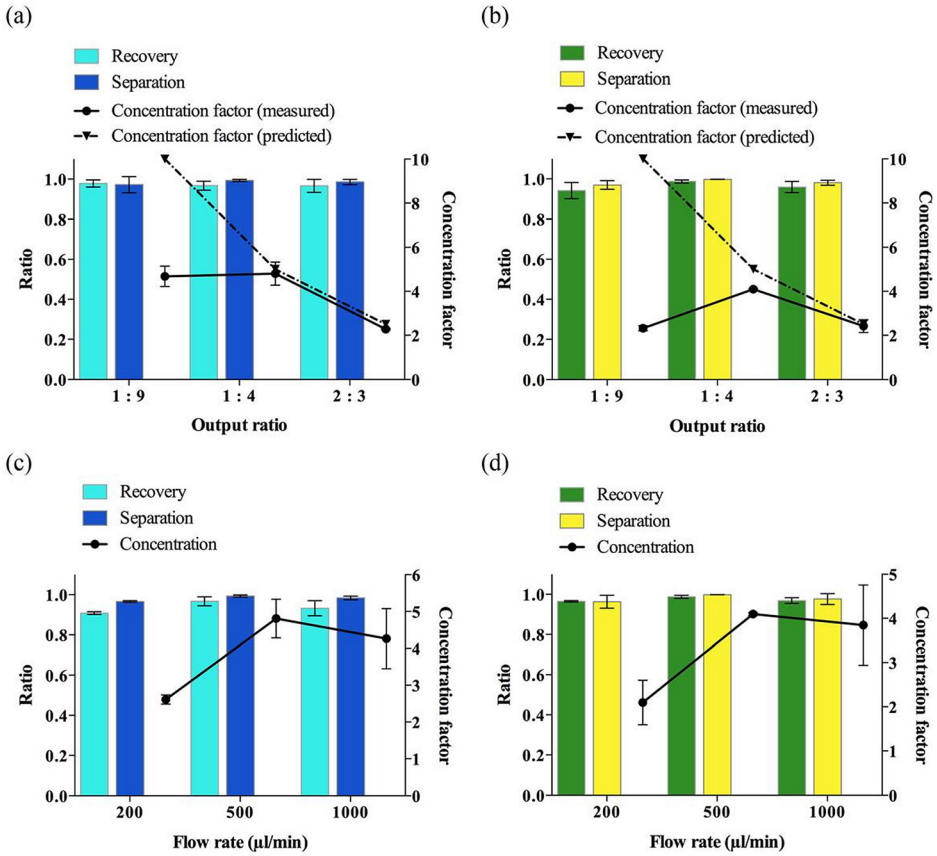

FIG. 4. Recovery ratio, separation ratio, and concentration factor at different output Q_{target} : Q_{waste} ratios and flow rates. The definitions of the recovery ratio, separation ratio, and concentration factor are given by Eqs. (3)–(5), respectively. PS particles (a) and *E. gracilis* cells (b) suspended in PBS. The discrepancy between the measured and theoretically predicted concentration factors is due to the central flow's weak drag force in the outlet tube at 50 μl/min in the case of the output flow ratio of 1:9. PS particles (c) and *E. gracilis* cells (d) suspended in PBS. The optimum conditions are an output ratio of 1:4 and 500 μl/min. The reason why the recovery ratio and hence the concentration factor are reduced at a high flow rate of 1000 μl/min is that the efficiency of focusing the particles and cells into the central acoustic pressure node is decreased due to their reduced retention time in the microchannel.

cannot be positioned in the highest velocity region of the parabolic flow profile in the target outlet tube where the drag force of the flow is not sufficient for them at a low flow rate of 40 μl/min (due to the output flow ratio of 1:4).

C. Enrichment of *E. gracilis*

Finally, to demonstrate the device's practical utility, we used a mixture of two different types of particles or cells to simulate a real sample. Specifically, we first used a mixture of 25-μm and 6-μm PS particles suspended in PBS to simulate a mixture of large and small microalgae. As shown in Fig. 5, the concentration factor of the large particles (2.06×10^5 particles/ml) from the mixture with the small particles (5.38×10^6 particles/ml) was measured to be 3.12 ± 0.40 with a recovery ratio of $95.0 \pm 2.6\%$, an enrichment factor of 15.30 ± 2.18, and a separation ratio of $93.4 \pm 1.8\%$. Next, we tested the device with a mixture of *E. gracilis* cells (1.02×10^5 cells/ml) and *M.* aff. *jurisii* cells (a smaller microalgal species of 3–4 μm in diameter, 1.22×10^7 cells/ml) suspended in PBS and obtained an concentration factor of 3.77 ± 0.29 with a recovery ratio of $93.6 \pm 1.9\%$, an enrichment factor of 10.16 ± 1.76, and a separation ratio of $89.0 \pm 0.8\%$ (Fig. 5).Finally, we used a sample of *E. gracilis* cells (2.1×10^5 cells/ml) spiked into pond water (GPS: 35°39′47.1″N 139°40′38.4″E, Komaba campus, University of Tokyo) to simulate an environmental sample and obtained an concentration

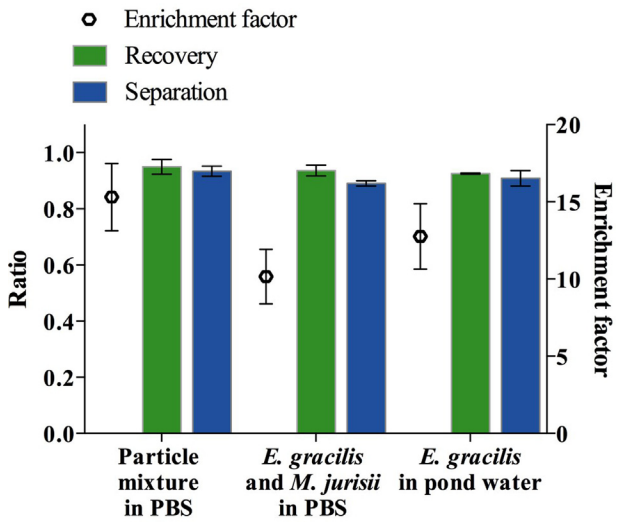

FIG. 5. Separation ratio, recovery ratio, and enrichment factor when mixtures of particles and cells were used. The definitions of the separation ratio, recovery ratio, and enrichment factor are given by Eqs. (3), (4), and (6), respectively. The left sample is a mixture of large and small particles suspended in PBS. The middle sample is a mixture of *E. gracilis* and *M.* aff. *jurisii* cells suspended in PBS. The right sample is *E. gracilis* cells spiked in pond water.

factor of 3.43 ± 0.26 with a recovery ratio of $92.6 \pm 0.2\%$, an enrichment factor of 12.76 ± 2.12, and a separation ratio of $90.1 \pm 2.7\%$ (Fig. 5) at a very high flow rate of 500 μl/min. Before spiking *E. gracilis* cells to the environmental pond water, large dust particles and pieces of leaves were removed by filtering the sample with a 40–μm nylon mesh to avoid clogging the microchannel. In these tests, the process of the alignment, separation, and enrichment did not affect the cell viability as shown in Fig. 6. The cell viability was found to be $98.3 \pm 0.7\%$ at a sample volume rate of 500 μl/min. The viability test was carried out by using a Neubauer chamber and 0.5% (w/v) vital dye calcein-AM with a volume of 10 μl for each sample. The results of the viability test show that the viability of the microalgal cells was not significantly affected by the acoustic waves and the temperature of the device. In case of operating the device for several hours, the temperature can be controlled by using a Peltier element on the device to prevent its temperature from rising. As Burguillos *et al.*[37] showed, the operation of acoustophoresis for over 48 h does not impact the survival, apoptosis, or proliferation of cells.

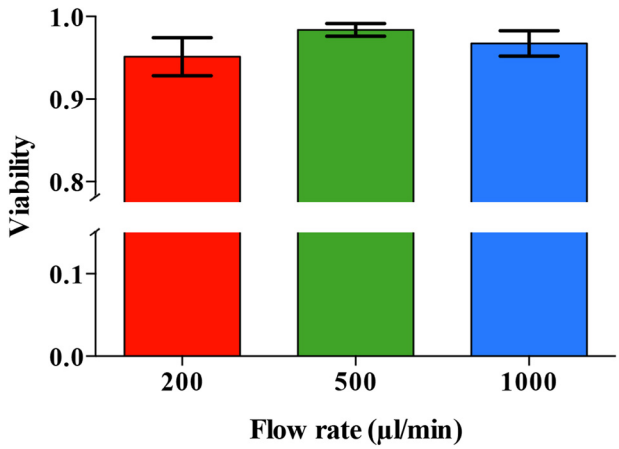

FIG. 6. Cell viability as a function of flow rate. The process of alignment, separation, and enrichment did not affect the cell viability. It was found to be 98.3% at a flow rate of 500 μl/min.

IV. CONCLUSIONS

We have proposed and experimentally demonstrated an on-chip acoustofluidic platform for harvesting a target microalgal species from a heterogeneous population of cells and particles based on their cellular size, density, and compressibility in a rapid, non-invasive, energy-efficient, continuously running, and automated manner. Our results indicate that the on-chip acoustofluidic platform is an effective tool for the simultaneous separation and enrichment of target microalgae from mixed populations of microalgae and other contaminants. Different from other harvesting methods such as filtration, chemical flocculation, and centrifugation, our method does not require any pre-treatment process and costly chemicals. However, since the method depends on the size, density, and compressibility of cells and particles, its applicability is limited to cells and particles that are similar in these parameters. While the throughput of a single device is limited to 30 ml/h, it can be significantly increased by using many devices in parallel, which is feasible due to the low cost of the device.

SUPPLEMENTARY MATERIAL

See supplementary material for visualization of the dynamics of the alignment, separation, and enrichment in the acoustofluidic device.

ACKNOWLEDGMENTS

This work was funded by the ImPACT Program of the Council for Science, Technology and Innovation (Cabinet Office, Government of Japan). *M*. aff. *jurisii* was kindly provided by Dr. Takashi Nakada from the Institute for Advanced Biosciences, Keio University. We are grateful to the members of Goda Lab for their assistance with our experiments.

[1]T. M. Mata, A. A. Martins, and N. S. Caetano, Renewable Sustainable Energy Rev. **14**, 217–232 (2010).
[2]Y. Chisti, Trends Biotechnol. **26**(3), 126–131 (2008).
[3]D. R. Georgianna and S. P. Mayfield, Nature **488**(7411), 329–335 (2012).
[4]R. H. Wijffels and M. J. Barbosa, Science **329**(5993), 796–799 (2010).
[5]Q. Hu, M. Sommerfeld, E. Jarvis, M. Ghirardi, M. Posewitz, M. Seibert, and A. Darzins, Plant J. **54**(4), 621–639 (2008).
[6]A. Kumar, S. Ergas, X. Yuan, A. Sahu, Q. O. Zhang, J. Dewulf, F. X. Malcata, and H. van Langenhove, Trends Biotechnol. **28**(7), 371–380 (2010).
[7]S. A. Scott, M. P. Davey, J. S. Dennis, I. Horst, C. J. Howe, D. J. Lea-Smith, and A. G. Smith, Curr. Opin. Biotechnol. **21**(3), 277–286 (2010).
[8]M. A. Carriquiry, X. D. Du, and G. R. Timilsina, Energy Policy **39**, 4222–4234 (2011).
[9]T. Mutanda, D. Ramesh, S. Karthikeyan, S. Kumari, A. Anandraj, and F. Bux, Bioresour. Technol. **102**(1), 57–70 (2011).
[10]B. Naveena, P. Armshaw, and J. T. Pembroke, Biotechnol. Biofuels **8**, 140 (2015).
[11]P. Spolaore, C. Joannis-Cassan, E. Duran, and A. Isambert, J. Biosci. Bioeng. **101**(2), 87–96 (2006).
[12]T. S. Sim, A. Goh, and E. W. Becker, Biomass **16**, 51–62 (1988).
[13]M. Olaizola, Biomol. Eng. **20**(4–6), 459–466 (2003).
[14]A. J. Dassey and C. S. Theegala, Bioresour. Technol. **128**, 241–245 (2013).
[15]R. Bhave, T. Kuritz, L. Powell, and D. Adcock, Environ. Sci. Technol. **46**(10), 5599–5606 (2012).
[16]G. P. Sheng, H. Q. Yu, and X. Y. Li, Biotechnol. Adv. **28**(6), 882–894 (2010).
[17]K. K. Sharma, S. Garg, Y. Li, A. Malekizadeh, and P. M. Schenk, Biofuels **4**(4), 397–407 (2014).
[18]A. Lenshof, M. Evander, T. Laurell, and J. Nilsson, Lab Chip **12**(4), 684–695 (2012).
[19]H. Mulvana, S. Cochran, and M. Hill, Adv. Drug Delivery Rev. **65**(11–12), 1600–1610 (2013).
[20]F. Petersson, A. Nilsson, C. Holm, H. Jonsson, and T. Laurell, Lab Chip **5**(1), 20–22 (2005).
[21]G. Destgeer and H. J. Sung, Lab Chip **15**, 2722–2738 (2015).
[22]H. Jönsson, C. Holm, A. Nilsson, F. Petersson, P. Johnsson, and T. Laurell, Ann. Thorac. Surg. **78**(5), 1572–1578 (2004).
[23]H. Inui, K. Miyatake, Y. Nakano, and S. Kitaoka, Eur. J. Biochem. **142**(1), 121–126 (1984).
[24]S. Koritala, J. Am. Oil Chem. Soc. **66**(1), 133–134 (1989).
[25]A. Ranjan, C. Patil, and V. S. Moholkar, Ind. Eng. Chem. Res. **49**(6), 2979–2985 (2010).
[26]G. S. Araujo, L. J. Matos, J. O. Fernandes, S. Cartaxo, L. Goncalves, F. Fernandes, and W. Farias, Ultrason. Sonochem. **20**(1), 95–98 (2013).
[27]M. Antfolk, P. B. Muller, P. Augustsson, H. Bruus, and T. Laurell, Lab Chip **14**(15), 2791–2799 (2014).
[28]S. Kato, Jap. J. Phycol **30**, 63–67 (1982) (in Japanese with English abstract).
[29]R. A. Andersen, J. A. Berges, P. J. Harrison, and M. M. Watanabe, *Algal Culturing Techniques* (Elsevier, Amsterdam, 2005), pp. 429–538.
[30]A. Nilsson, F. Petersson, H. Jonsson, and T. Laurell, Lab Chip **4**(2), 131–135 (2004).
[31]J. W. Judy, Smart Mater. Struct. **10**, 1115–1134 (2001).
[32]T. Laurell, F. Petersson, and A. Nilsson, Chem. Soc. Rev. **36**(3), 492–506 (2007).
[33]J. H. Jung, K. S. Lee, S. Im, G. Destgeer, B. H. Ha, J. Park, and H. F. Sung, RSC Adv. **6**, 11081–11087 (2016).

[34]C. Grenvall, J. R. Folkenberg, P. Augustsson, and T. Laurell, Cytometry, Part A **81A**(12), 1076–1083 (2012).
[35]O. Jakobsson, C. Grenvall, M. Nordin, M. Evander, and T. Laurell, Lab Chip **14**(11), 1943–1950 (2014).
[36]C. Grenvall, P. Augustsson, J. R. Folkenberg, and T. Laurell, Anal. Chem. **81**(15), 6195–6200 (2009).
[37]M. Burguillos, C. Magnusson, M. Nordin, A. Lenshof, P. Augustsson, M. J. Hansson, E. Elmer, H. Lilja, P. Brundin, T. Laurell, and T. Deierborg, PLoS One **8**(5), e64233 (2013).